Progress of Theoretical Physics, Vol. 57, No. 6, June 1977

Nonstatic One-Boson-Exchange Potential with Retardation and Nuclear Matter

——*Including Velocity-Dependent Tensor Potential*——

Toshio OBINATA and Masanobu WADA

The Physical Science Laboratories, College of Science and Technology
Nihon University, Funabashi 274

(Received November 4, 1976)

Several kinds of phase-shift equivalent one-boson-exchange potential (OBEP) including velocity-dependent term are constructed so as to reproduce the two-nucleon data. Here we propose an "extended Green's method" to treat the velocity-dependent tensor potential. Nuclear matter and neutron matter properties are calculated for our nonstatic OBEP. The phase-shift equivalent OBEP's, however, give different nuclear matter properties owing to the difference of the softness of core potential and the retardation. The retardation strengthens the tensor-to-central ratio of OBEP in the triplet even state, and reduces the nuclear matter binding energy per particle by 2.6~5.0 MeV with a decrease in density by 0.05~0.08 fm^{-1}. However, the retarded effect on neutron matter is relatively small.

§ 1. Introduction

The retardation is an important part of the nonstatic effects of meson theoretical nucleon-nucleon potentials. Since many-nucleon systems are susceptible to the off-energy-shell elements of the potentials coming from the retardation, the retarded effects in these systems are expected to be more important than that in two-nucleon systems. By this reason, the retarded effects in nuclear structure studies are of great interest.

In previous papers[1),2)] (hereafter referred to as I and II, respectively), we attempted to construct the nonstatic OBEP with retardation in r-space for the sake of future applications to finite nuclei, and to elucidate the retarded effect on nuclear matter. Strictly speaking, the treatment of nonstatic effects in these analyses were, however, insufficient because the velocity-dependent tensor term of the OBEP was disregarded.

The aim of this paper is to reconstruct the OBEP including the velocity-dependent tensor part and to examine the properties of both nuclear and neutron matters for this OBEP.

The velocity-dependent tensor potential complicates the treatment of the Schrödinger equation in an usual manner. But if we use the "extended Green's method",[3)] it is possible to handle the problem easily in the same way as the velocity-independent case.

As is seen in the later part of this paper, some improvements in the meson parameters of OBEP to fit the experimental data are resulted by the inclusion of the velocity-dependent tensor potential. The retarded effect on saturation properties of nuclear matter, by which the binding energy and saturation density are reduced as was clarified in II, tends to be enhanced by this nonstatic tensor term. Besides, the analysis of neutron matter shows that the retarded effect in this system is relatively small in spite of its high density.

In § 2, brief discussion of the r-space OBEP and the phenomenological treatment of the core region are given. Several kinds of OBEP including the velocity-dependent tensor term are constructed so as to fit the experimental two-nucleon data. In § 3, by the applications of these OBEP's to the nuclear matter and neutron matter, the retarded effects in both systems are investigated.

§ 2. Analysis of two-nucleon systems with the retarded OBEP

2.1. *Potential*

The derivation of the r-space OBEP with retardation was shown in I. The detailed forms from the exchange of the scalar, pseudoscalar and vector mesons are summarized in the Appendix.

For the definition of the nucleon-meson coupling constants, we show the interaction Lagrangian densities:

$$L_s' = \sqrt{4\pi} g_s \bar{\psi}\psi\phi^{(s)}\,, \tag{2·1a}$$

$$L_p' = \sqrt{4\pi}\left\{g_p \bar{\psi} i\gamma_5 \psi\phi^{(p)} + \frac{f_p}{m_p}\bar{\psi} i\gamma_5\gamma_\mu \partial_\mu \phi^{(p)}\right\}, \tag{2·1b}$$

$$L_v' = \sqrt{4\pi}\left\{g_v \bar{\psi} i\gamma_\mu \psi\phi_\mu^{(v)} + \frac{f_v}{2m_v}\bar{\psi}\sigma_{\mu\nu}\psi\phi_{\mu\nu}^{(v)}\right\}, \tag{2·1c}$$

$$\sigma_{\mu\nu} = (\gamma_\mu\gamma_\nu - \gamma_\nu\gamma_\mu)/2i\,, \quad \phi_{\mu\nu} = \partial_\mu\phi_\nu - \partial_\nu\phi_\mu\,, \tag{2·2}$$

where $m_i (i = p, v)$ are meson masses.

The general form of r-space potential is represented as

$$V = U_C + U_T S_{12} + U_{LS}(\boldsymbol{L}\cdot\boldsymbol{S}) + U_W W_{12} + U_{LL}\boldsymbol{L}^2\,, \tag{2·3}$$

where S_{12} is the usual tensor operator and

$$W_{12} = \{(\boldsymbol{\sigma}_1\cdot\boldsymbol{L})(\boldsymbol{\sigma}_2\cdot\boldsymbol{L}) + (\boldsymbol{\sigma}_2\cdot\boldsymbol{L})(\boldsymbol{\sigma}_1\cdot\boldsymbol{L})\}/2 - (\boldsymbol{\sigma}_1\cdot\boldsymbol{\sigma}_2)\boldsymbol{L}^2/3\,. \tag{2·4}$$

The function U_i of our OBEP consists of two parts:

$$U_i = V_i + W_i\,, \quad i = (C, T, LS, W, LL), \tag{2·5}$$

where V_i and W_i are the usual Yukawa and the retarded potentials, respectively. The detailed forms of V_i and W_i are given in the Appendix.

Since the nuclear interaction in the core region seems to be beyond the

applicability of the OBE model, we introduce the phenomenological core potential $V_{\rm core}$ and a cutoff function $F_i(r)$ to suppress the contribution of Eq. (2·3),

$$F_i(r)=\{1-\exp[-(r/\eta_{\rm cut})^2]\}^{n_i}, \quad i=(C, T, LS, W, LL). \tag{2·6}$$

The phenomenological core potential consists of the repulsive central and attractive LS terms.[4] The repulsive core is introduced to reproduce the S state phase shifts, and the attractive LS core to improve the ${}^3P_J$ state phase shifts.

$$V_{\rm core}=V^C_{\rm core}(r)+V^{LS}_{\rm core}(r)\,(\boldsymbol{L}\cdot\boldsymbol{S}). \tag{2·7}$$

The following three types are assumed for $V_{\rm core}$.

1) OBEH; hard core plus LS core:

$$V^C_{\rm core}(r)=\begin{cases}\infty\,; r\leqq r_c\,,\\ 0\,; r>r_c\,,\end{cases} \tag{2·8}$$

$$V^{LS}_{\rm core}(r)=-V_{LS}\exp[-(r/\eta_{LS})^2]. \tag{2·9}$$

2) OBEG; the Gaussian soft core plus the Thomas type LS core:

$$V^C_{\rm core}(r)=V_G\exp[-(r/\eta_G)^2], \tag{2·10}$$

$$V^{LS}_{\rm core}(r)=\frac{1}{M^2}\cdot\frac{1}{r}\cdot\frac{\partial V^C_{\rm core}(r)}{\partial r}\,. \tag{2·11}$$

3) OBEV; velocity-dependent core plus LS core:

$$V^C_{\rm core}(r)=\{\boldsymbol{p}^2\phi(r)+\phi(r)\boldsymbol{p}^2\}/M, \quad \phi(r)=\phi_p\exp[-(r/\eta_p)^2], \tag{2·12}$$

$$V^{LS}_{\rm core}(r)=-V_{LS}\exp[-(r/\eta_{LS})^2]. \tag{2·13}$$

2.2. *Inclusion of the velocity-dependent tensor potential*

The tensor potentials of the OBEP's from the pseudoscalar meson and vector meson (tensor coupling) depend partly on the velocity as is shown in the Appendix. We will attempt to construct the net OBEP including these velocity-dependent tensor potentials in addition to the other nonstatic terms. This task is easily performed by the "extended Green's method".[3]

We assume the following potential form:

$$V=U(r)-\frac{1}{M}(\boldsymbol{\nabla}^2\phi_c(r)+\phi_c(r)\boldsymbol{\nabla}^2)-\frac{1}{M}(\boldsymbol{\nabla}^2\phi_T(r)S_{12}+\phi_T(r)S_{12}\boldsymbol{\nabla}^2), \tag{2·14}$$

where $U(r)$ stands for the velocity-independent potential. The coupled equation with the potential (2·14) is written in matrix form as

$$\begin{pmatrix}D_c-\alpha^{J-1}D_T & \alpha^{ND}D_T\\ \alpha^{ND}D_T & D_c-\alpha^{J+1}D_T\end{pmatrix}\begin{pmatrix}u_J\\ w_J\end{pmatrix}=\begin{pmatrix}A^{J-1} & A^{ND}\\ A^{ND} & A^{J+1}\end{pmatrix}\begin{pmatrix}u_J\\ w_J\end{pmatrix}, \tag{2·15}$$

where

$$D_c=(1+2\phi_c(r))\frac{d^2}{dr^2}+2\frac{d\phi_c(r)}{dr}\cdot\frac{d}{dr}+\frac{d^2\phi_c(r)}{dr^2}+k^2\,, \tag{2·16}$$

$$D_T = 2\phi_T(r)\frac{d^2}{dr^2} + 2\frac{d\phi_T(r)}{dr}\cdot\frac{d}{dr} + \frac{d^2\phi_T(r)}{dr^2}, \tag{2·17}$$

$$\alpha^{J-1} = \frac{2(J-1)}{2J+1}, \quad \alpha^{J+1} = \frac{2(J+2)}{2J+1}, \quad \alpha^{ND} = \frac{6\sqrt{J(J+1)}}{2J+1}, \tag{2·18}$$

$$A^{J\pm1} = (1 + 2\phi_c(r) - 2\alpha^{J\pm1}\phi_T(r))\frac{(J\pm1)(J+1\pm1)}{r^2} + MU_{J\pm1}, \tag{2·19}$$

$$A^{ND} = \alpha^{ND}\left(2\phi_T(r)\frac{(J^2+J+1)}{r^2} + MU_T\right). \tag{2·20}$$

Here, $U_{J\pm1}$ denotes the effective potential for the $L=J\pm1$ state, and U_T is the tensor potential of $U(r)$. The differential operator D_T appeared in nondiagonal part of the left-hand side of Eq. (2·15) obstructs straightforward application of the "Green's method".

The diagonalization of the left-hand side of Eq. (2·15) is performed by a unitary matrix as

$$R = \begin{pmatrix} \cos\theta & \sin\theta \\ -\sin\theta & \cos\theta \end{pmatrix}. \tag{2·21}$$

The diagonalization is obtained when $\cos\theta = \sqrt{(J+1)/2J+1}$ and $\sin\theta = \sqrt{J/2J+1}$. Then we obtain a new coupled equation as follows:

$$\begin{pmatrix} D^{J-1} & 0 \\ 0 & D^{J+1} \end{pmatrix}\begin{pmatrix} f_J \\ g_J \end{pmatrix} = \begin{pmatrix} 0 & V_{ND} \\ V_{ND} & 0 \end{pmatrix}\begin{pmatrix} f_J \\ g_J \end{pmatrix}, \tag{2·22}$$

where

$$D^{J\pm1} = \frac{d^2}{dr^2} + k^2 - \frac{(J\pm1)(J+1\pm1)}{r^2} - V_{J\pm1}, \tag{2·23}$$

$$V_{J\pm1} = \frac{M}{1+2\phi_{J\pm1}}\left\{\frac{J+1}{2J+1}U_{J\pm1} + \frac{J}{2J+1}U_{J\mp1} \mp \frac{12J(J+1)}{(2J+1)^2}U_T\right\} - \frac{(d\phi_{J\pm1}/dr)^2}{(1+2\phi_{J\pm1})^2} + \frac{2\phi_{J\pm1}}{1+2\phi_{J\pm1}}\cdot k^2 \mp \frac{2J}{r^2}, \tag{2·24}$$

$$V_{ND} = \frac{M}{\sqrt{(1+2\phi_{J+1})(1+2\phi_{J-1})}}\cdot\frac{6\sqrt{J(J+1)}}{2J+1}\left\{\frac{1}{6}(U_{J+1} - U_{J-1}) + \frac{1}{2J+1}U_T + \frac{1}{3}(1+\phi_{J+1}+\phi_{J-1})\frac{2J+1}{r^2}\right\}, \tag{2·25}$$

$$\phi_{J+1} = \phi_C(r) - 4\phi_T(r), \quad \phi_{J-1} = \phi_C(r) + 2\phi_T(r). \tag{2·26}$$

The solutions of Eq. (2·22), f_J and g_J are related to the original wave functions, u_J and w_J as

$$\begin{pmatrix} u_J \\ w_J \end{pmatrix} = \begin{pmatrix} \sqrt{(J+1)/2J+1} & -\sqrt{J/2J+1} \\ \sqrt{J/2J+1} & \sqrt{(J+1)/2J+1} \end{pmatrix} \begin{pmatrix} f_J/\sqrt{1+2\phi_{J-1}} \\ g_J/\sqrt{1+2\phi_{J+1}} \end{pmatrix}. \quad (2\cdot27)$$

It is to be noticed that a condition as $1+2\phi_{J\pm1}\neq0$ must be guaranteed for an application of the "extended Green's method".

2.3. *Fits to two-nucleon data*

In this subsection, we will search for the parameters of the net OBEP that reproduce the scattering phase shifts, the two-nucleon low energy parameters and the deuteron properties.

In addition to the exchange of well-established π, η, ω and ρ mesons, two hypothetical scalar mesons $\sigma_0(I, J^\pi=0, 0^+)$ and $\sigma_1(1, 0^+)$ are introduced. σ_1 meson ensure the state-independency of central core potential. The detailed discussion on the meson parameters was made in I, provided that the isovector-scalar meson was called δ instead of σ_1 used in this paper.

The reduction parameter $\lambda=0.5$ is multiplied by the nonstatic terms of order p^2/M^2. The cutoff radius in Eq. (2·6) is taken as $\eta_{\text{cut}}=0.36$ fm for OBEH and

Table I. Potential parameters of the r-space OBEP's. Inner potential parameters are common to both (R) and (NR). For the potential names, refer to the text. Meson masses are fixed as $m_\pi=139$ MeV, $m_\eta=549$ MeV, $m_{\sigma_0}=550$ MeV, $m_{\sigma_1}=770$ MeV, $m_\omega=784$ MeV and $m_\rho=765$ MeV for all kinds of potential.

	OBEG (R)-SC	OBEG (NR)-SC	OBEG (R)-LC	OBEG (NR)-LC	OBEV (R)	OBEV (NR)	OBEH (R)	OBEH (NR)
Meson const								
g_π^2	13.5	13.5	13.5	13.5	13.5	13.5	13.5	13.5
g_η^2	2.0	2.0	2.0	2.0	2.0	2.0	2.0	2.0
$g_{\sigma_0}^2$	8.88	9.0	8.75	9.14	7.33	7.98	8.12	8.4
$g_{\sigma_1}^2$	2.396	2.14	2.805	2.77	1.53	1.52	3.39	3.305
g_ω^2	18.0	17.0	13.5	13.0	17.0	16.9	16.0	15.1
g_ρ^2	0.93	1.0	0.9	1.05	0.88	0.93	1.0	1.2
(f_ρ/g_ρ)	1.57	1.85	1.5	1.65	1.38	1.5	1.63	1.76
λ	0.5	0.5	0.5	0.5	0.5	0.5	0.5	0.5
η_{cut}(fm)	0.36	0.36	0.36	0.36	0.5	0.5	0.36	0.36
Central core								
r_c(fm)	—		—		—		0.36	
η_G(fm)	0.36		0.58		—		—	
V_G(GeV)	2.8		0.65		—		—	
η_p(fm)	—		—		0.6		—	
ϕ_p	—		—		1.1		—	
LS core	Thomas term		Thomas term					
η_{LS}(fm)	—		—		0.6		0.45	
V_{LS}(GeV)	—		—		−0.65		−2.0	

OBEG and $\eta_{\rm cut}=0.5$ fm for OBEV. The exponents n_i are fixed as 5 for $i=C$, T, LS and 6 for $i=W$, LL.

Essentially free parameters of our OBEP are $g^2_{\sigma_0}$, $g^2_{\sigma_1}$, $g_\omega{}^2$, $g_\rho{}^2$, $(f/g)_\rho$, m_{σ_0} and m_{σ_1} in addition to the inner potential parameters. The parameters obtained from the search are listed in Table I.

The four kinds of OBEP are considered here, viz., the OBEH, OBEV and two kinds of OBEG with small core radius (OBEG-SC) and large core radius (OBEG-LC). We use henceforce the abbreviations (R) and (NR) for the potentials with and without retardation, respectively. For instance, the OBEG with retardation and small core radius is referred to as OBEG(R)-SC.

As is seen in Table I, the coupling constant of ω meson for (NR) is smaller than that for (R), and conversely in the case of σ_0 meson, the coupling constant for (NR) is larger than that for (R). These tendencies are due to the attractive character of retarded effect of the OBEP on nucleon-nucleon scattering.[5]

Since the retarded effects of π and η meson exchange are small, the π-N and η-N coupling constants for (R) and (NR) are taken as a common value. In the case of ρ meson, both $g_\rho{}^2$ and $(f/g)_\rho$ for (R) are smaller than those for (NR). This change of the coupling constant is effective to strengthen the tensor part of (R) in the triplet even state. As compared with the results in I, the coupling constants of σ_0, σ_1 and ω mesons are slightly reduced, but that of ρ meson is made somewhat larger one by inclusion of the velocity-dependent tensor terms. However, $g^2_{\sigma_0}$ and $g_\omega{}^2$ are somewhat larger than those of the OBEP's by other authors.

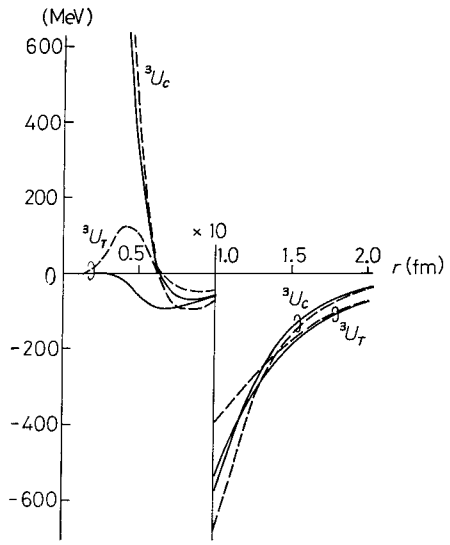

Fig. 1. The central and tensor potentials in the ^3E state for the cases of OBEG(R)-SC (solid curves) and OBEG(NR)-SC (dashed curves).

(i) Potentials

Characteristics of the OBEP are almost the same as those obtained in I. In Fig. 1, the central and tensor potentials in the triplet even (^3E) state for the case of OBEG-SC are shown. The tensor-to-central ratio U_T/U_C of (R) in the ^3E state is larger than that of (NR) in the intermediate region as in Fig. 1. This is due to the smaller ρ-N coupling constant for (R) than that for (NR), and is an important character of the retarded effects for nuclear matter calculations. Yet the OBEV is the smoothest, the features of all the OBEP's are almost the same as one another, except for a small reformation in the core region. For each type of core potential, the difference between (R) and (NR) is relatively large

on the potentials in the intermediate region, especially on the quadratic LS and L^2 potentials.

Both potentials (R) and (NR) are typical examples of phase shift equivalent potentials that differ from each other in the potential shapes.

(ii) Scattering phase shifts

Hereafter, we treat OBEG(R)-SC as our standard soft core potential because of considering the off-energy-shell property and yielding proper nuclear matter binding energy. We use the expression OBEG instead of OBEG-SC unless otherwise noticed. The phase shifts calculated from OBEG are exhibited in Figs. 2, 3 and 4 (other potentials give somewhat the same results). An overall fit is fairly good. The error bars in figures are the experimental values given by Arndt, MacGregor and Wright.[6]

The retardation gives large additional attraction, mainly in the $^1S_0$ and $^3S_1$ states as shown in Figs. 2 and 3, in which dash-dotted curves are obtained by omitting the retardation in OBEG(R). This tendency is qualitatively in agreement with that of p-space calculations.[5),7)]

Effects of tensor potential in the $^3S_1$ state are shown in Fig. 3 by dotted curves. Static tensor potential omitted velocity-dependent terms gives a large attractive contribution. However, effects of velocity-dependent tensor terms are repulsive.

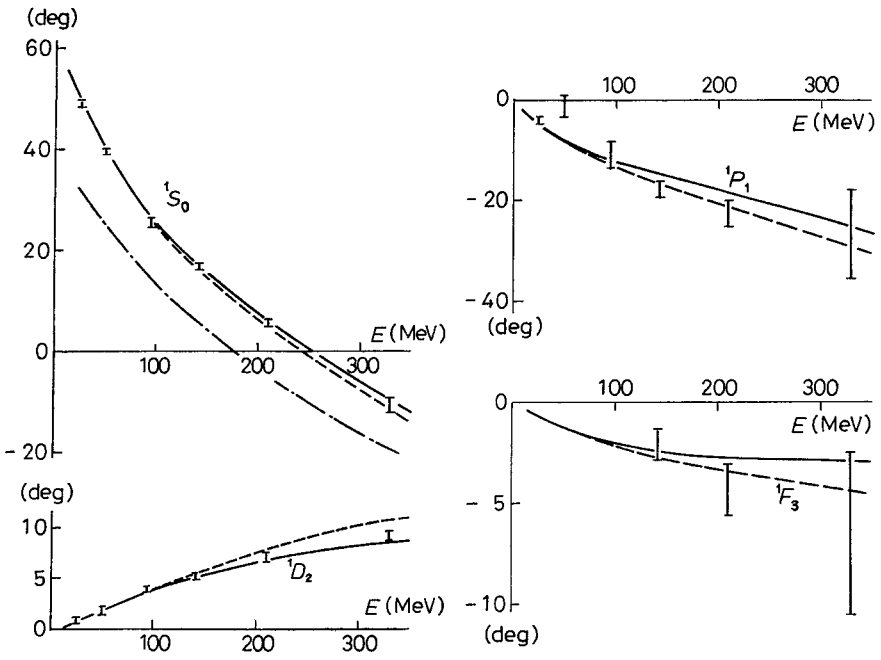

Fig. 2. The ^1E and ^1O phase shifts calculated from OBEG(R) (solid curves) and OBEG(NR) (dashed curves). The dash-dotted curve represents the result when omitting the retarded part of OBEG(R).

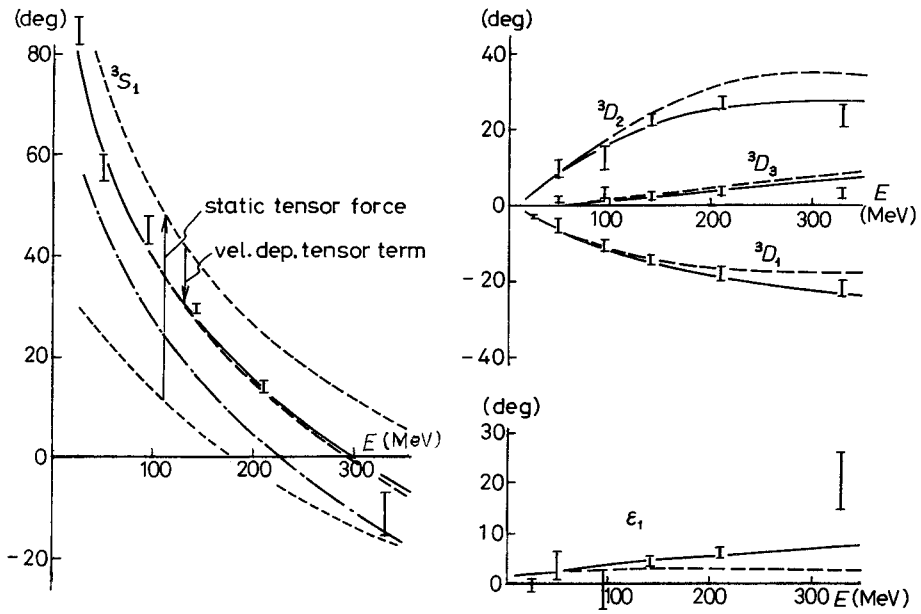

Fig. 3. The same as in Fig. 2 but for the ^3E phase shifts. The arrows indicate the contributions from both static and velocity-dependent tensor terms of OBEG(R)-SC.

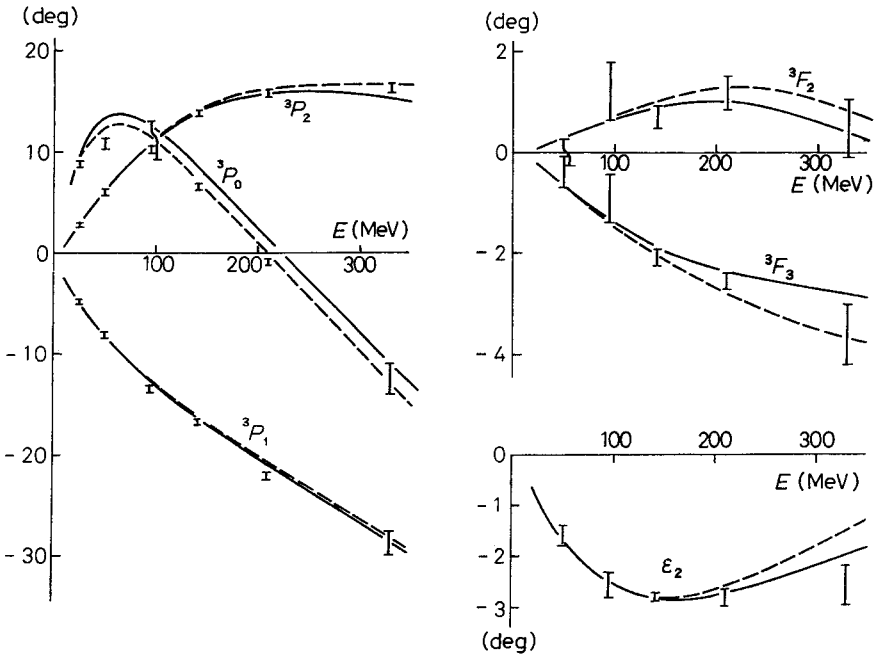

Fig. 4. The same as in Fig. 2 but for the ^3O phase shifts.

As compared with I, appreciable improvements to the ${}^3S_1+{}^3D_1$ and ${}^3P_J$ states are achieved by inclusion of velocity-dependent tensor terms and phenomenological LS core potential. However, the ${}^3P_0$ phase shift at lower energies is still larger than the experimental one. The discrepancies, especially in the ${}^3P_2$, ε_1 at high energies are yet remained.

The χ^2-quantity is defined as

$$\chi^2=\sum_{\text{phase}}\left(\frac{\delta_i^{\text{th}}-\delta_i^{\text{exp}}}{\Delta\delta_i^{\text{exp}}}\right)^2,$$

where the δ_i^{th} are the theoretical phase shifts, the δ_i^{exp} experimental phase shifts and the $\Delta\delta_i^{\text{exp}}$ errors assigned to δ_i^{exp}. Here we use the Livermore analysis at 25, 50, 95, 142, 210 and 330 MeV (86 pieces of data) as the δ_i^{exp}.

The χ^2 values of OBEG are 6.5 and 6.4 for (R) and (NR), respectively, compared to 14.3 and 15.0 obtained by OBEG without velocity-dependent tensor terms. This improvement in data fit seems due to the velocity-dependent tensor terms and phenomenological LS core potential.

(iii) Low energy parameters and deuteron properties

The low energy parameters and deuteron properties calculated from four kinds

Table II. Low energy parameters and deuteron properties. For the singlet state, values in p-p scattering are shown. The quantities contained within parentheses are values from the same OBEP's without the Coulomb force.

	${}^1r_e$(fm)	${}^1a$(fm)	${}^3r_e$(fm)	${}^3a$(fm)	E_d(MeV)	Q_d(fm^2)	P_D (%)
OBEG(R)-SC	2.61 (2.68)	−7.71 (−17.4)	1.801	5.50	2.2239	0.2763	5.12
OBEG(NR)-SC	2.63 (2.71)	−7.78 (−17.5)	1.819	5.46	2.2266	0.2634	4.18
OBEG(R)-LC	2.59 (2.65)	−7.54 (−16.9)	1.782	5.47	2.2223	0.2736	5.06
OBEG(NR)-LC	2.62 (2.69)	−7.70 (−17.4)	1.792	5.44	2.2250	0.2620	4.21
OBEV(R)	2.57 (2.64)	−7.67 (−17.5)	1.791	5.46	2.2219	0.2662	4.22
OBEV(NR)	2.61 (2.68)	−7.67 (−17.3)	1.808	5.45	2.2232	0.2611	4.00
OBEH(R)	2.61 (2.69)	−7.76 (−17.5)	1.791	5.46	2.2273	0.2711	4.75
OBEH(NR)	2.65 (2.74)	−7.75 (−17.2)	1.794	5.42	2.2245	0.2538	3.65
Exp	2.794[a] ±0.015 (2.84 ±0.03)	−7.823[a] ±0.01 (−17.0 ±1)	1.750[b] ±0.005	5.414[b] ±0.005	2.2245[c] ±0.0002	0.278[b] ±0.008	—

a) H. P. Noyes and H. M. Lipinski, Phys. Rev. **C4** (1971), 995.

b) E. Lommon and R. Wilson, Phys. Rev. **C9** (1974), 1329.

c) R. Wilson, *The nucleon-nucleon interaction* (Interscience Publishers, Wiley, N. Y. and London, 1963).

of OBEP are shown in Table II. All kinds of potential give nearly the same values, however, (R) give a large quadrupole moment and large D-state probability in comparison with those from (NR). It indicates the strong tensor potential of (R) in the ^3E state.

§ 3. Nuclear matter and neutron matter

3.1. *Calculational method*

Our calculational method is based on the p-space formalism of the Brueckner theory by Harada, Tamagaki and Tanaka.[8] For detail of this method, we described in II. Here we give merely some comments. The Bethe-Goldstone equation is written as

$$\langle \boldsymbol{m}_0\boldsymbol{n}_0|G|\boldsymbol{m}_0\boldsymbol{n}_0\rangle = \langle \boldsymbol{m}_0\boldsymbol{n}_0|v|\boldsymbol{m}_0\boldsymbol{n}_0\rangle + \int\int d\boldsymbol{m}_1 d\boldsymbol{n}_1 \langle \boldsymbol{m}_0\boldsymbol{n}_0|v|\boldsymbol{m}_1\boldsymbol{n}_1\rangle \frac{Q}{e(\Sigma, \boldsymbol{m}_1, \boldsymbol{n}_1)} \langle \boldsymbol{m}_1\boldsymbol{n}_1|G|\boldsymbol{m}_0\boldsymbol{n}_0\rangle , \tag{3·1}$$

$$e(\Sigma, \boldsymbol{m}_1, \boldsymbol{n}_1) = \Sigma - E_l(\boldsymbol{m}_1) - E_l(\boldsymbol{n}_1), \tag{3·2}$$

where Σ is the starting energy and E_l is the single particle energy for which the potential energy is neglected according to the hole line expansion.[9] The potential energy is given as

$$U_0(\boldsymbol{m}_0) = \sum_{|\boldsymbol{n}_0|<k_F} \langle \boldsymbol{m}_0\boldsymbol{n}_0|G|\boldsymbol{m}_0\boldsymbol{n}_0 - \boldsymbol{n}_0\boldsymbol{m}_0\rangle . \tag{3·3}$$

The total energy per particle is

$$\frac{E}{A} = \int_0^{k_F} dm_0 m_0^2 \left[T(m_0) + \frac{1}{2} U_0(m_0) \right] \Big/ \int_0^{k_F} dm_0 m_0^2 , \tag{3·4}$$

where $T(m_0)$ is the nonrelativistic kinetic energy. The binding energy denotes the absolute value of the total energy.

The defect wave function $F_{l'l}^{(JST)}$ and the wound integral $\kappa_{l'l}^{(JST)}$ for each partial wave are represented in momentum space as follows:

$$F_{l'l}^{(JST)}(k, k_0; P) = \frac{k\bar{Q}(k, P) G_{l'l}^{(JST)}(k, k_0; P)}{e(\Sigma, k, P)} , \tag{3·5}$$

$$\kappa_{l'l}^{(JST)}(k_0; P) = \frac{n k_F^3}{3\pi^2} (2J+1)(2T(n-1)+1) \int_0^\infty dk |F_{l'l}^{(JST)}(k, k_0; P)|^2 , \tag{3·6}$$

$$\boldsymbol{k} = (\boldsymbol{m} - \boldsymbol{n})/2 , \quad \boldsymbol{P} = (\boldsymbol{m} + \boldsymbol{n})/2 , \tag{3·7}$$

where $n=2$ for nuclear matter and $n=1$ for neutron matter, $\boldsymbol{k}$ and $\boldsymbol{k}_0$ are relative momentum of the two nucleons in intermediate and initial states, respectively, and $\boldsymbol{P}$ is the c.m. momentum.

3.2. *Nuclear matter properties*

Saturation curves for each kind of soft core OBEP are shown in Fig. 5(a).

Partial wave contributions for OBEG-SC are exhibited in Fig. 5(b) and Table III. Binding energies per particle at saturation densities are listed in Table IV.

The large discrepancy of the saturation points between OBEG-SC and OBEV (-15.6 MeV (1.64 fm^{-1}) to -24.2 MeV (1.83 fm^{-1})) is completely due to the dif-

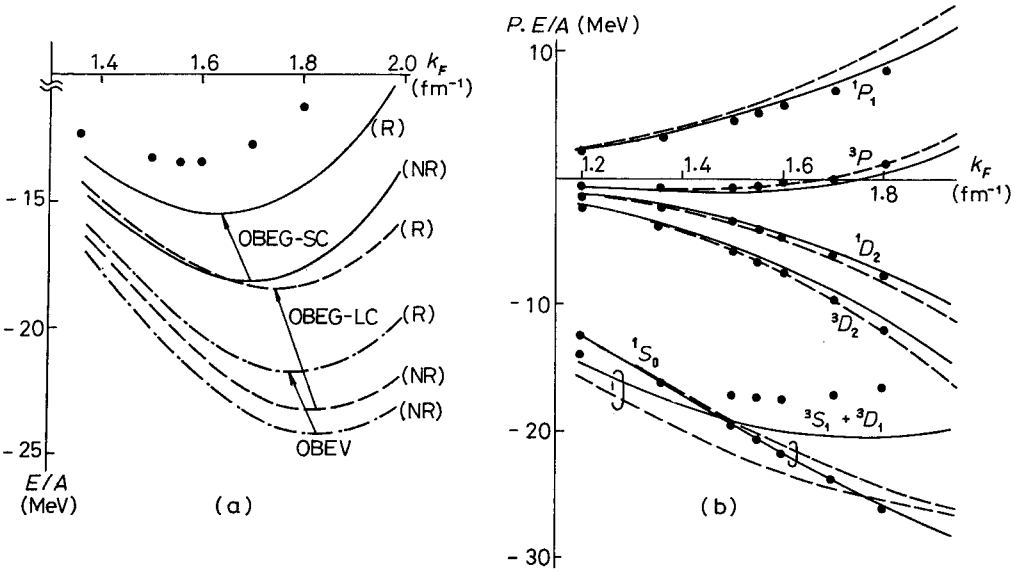

Fig. 5. Saturation curves in case of (R) and (NR) are shown in (a). Partial wave contributions from OBEG(R)-SC (solid curves) and OBEG(NR)-SC (dashed curves) are shown in (b). The dots · show the value from p-space OBEP.[11]

Table III. Partial wave contributions to the potential energy (MeV/A) at $k_F=1.6$ fm^{-1} for each kind of soft core OBEP.

	OBEG(R) -SC	OBEG(NR) -SC	OBEG(R) -LC	OBEG(NR) -LC	OBEV(R)	OBEV(NR)
$^1S_0$	−21.64	−20.84	−22.88	−22.24	−22.91	−22.57
$^1P_1$	6.09	6.90	6.14	6.71	5.09	5.34
$^1D_2$	−4.37	−4.78	−4.30	−4.75	−3.86	−4.27
$^3S_1$	−22.35	−25.61	−23.80	−26.36	−26.09	−26.49
$^3D_1$	2.46	2.46	2.49	2.52	2.66	2.79
$^3D_2$	−6.94	−7.51	−6.89	−7.50	−6.70	−7.28
$^3D_3$	0.20	0.18	0.21	0.18	0.14	0.13
$^3P_0$	−5.22	−4.95	−5.45	−5.35	−4.57	−4.77
$^3P_1$	18.12	18.25	18.36	18.26	19.38	19.41
$^3P_2$	−13.79	−13.69	−13.38	−14.27	−15.13	−16.05
Pot. energy	−47.43	−49.60	−49.49	−52.80	−52.00	−53.77
Kin. energy	31.85	31.85	31.85	31.85	31.85	31.85
Bind. energy	15.58	17.75	17.65	20.95	21.15	21.92

Table IV. Saturation properties for each kind of OBEP.

Potential	Density in k_F (fm^{-1})	Bind. energy (MeV/A)
OBEG(R)-SC	1.64	15.6
OBEG(NR)-SC	1.70	18.2
OBEG(R)-LC	1.75	18.4
OBEG(NR)-LC	1.83	23.4
OBEV(R)	1.78	21.7
OBEV(NR)	1.83	24.2

ference in the softness of core potential and the weakness of tensor potential.[10] The results predicted by OBEG(R)-SC are considerably better than those given by other potentials, and in relatively good agreement with those obtained from the p-space calculation by Holinde et al.[11] Both OBEG-LC and OBEV produce the overbinding. Thus they seem to be an inappropriate potential.

The binding energy and saturation density produced by (R) are small compared with those by (NR) due to the large D-state probability. This tendency is qualitatively independent of the type of core potential.

It is easily seen that the difference of the binding energies between (R) and (NR) arises mainly from the ${}^3S_1+{}^3D_1$ states sensitively reflected the difference of tensor-to-central ratios between (R) and (NR). Also the effect of retardation seems to be rather enhanced by inclusion of the velocity-dependent tensor terms in comparison with II.

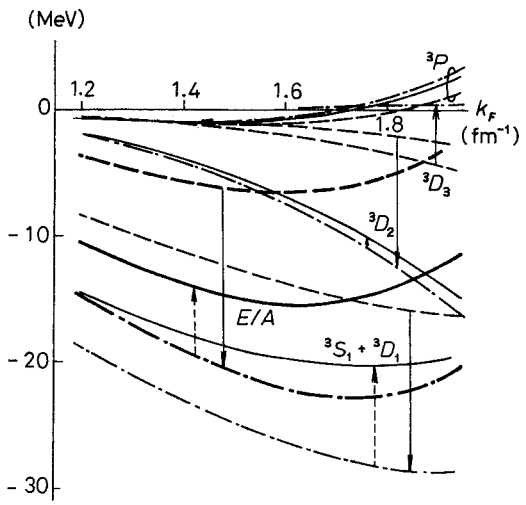

Fig. 6. Solid curves indicate partial wave contributions from OBEG(R). Dashed curves and dash-dotted curves show the results from OBEG(R) omitting all tensor potentials and OBEG(R) omitting only the velocity-dependent tensor terms, respectively.

Each effect omitting the tensor potential and only the velocity-dependent tensor terms is shown in Fig. 6 by dotted line. The contribution of the static tensor potential is attractive and large for the ${}^3S_1+{}^3D_1$ and ${}^3D_2$ states, while a net contribution for the ${}^3P_J$ states is very small. The velocity-dependent tensor terms contribute repulsively to the ${}^3S_1+{}^3D_1$ states. The tendencies above mentioned are similar to that of phase shifts.

In Table V, wound integrals $\kappa_{l'l}^{(JST)}$ of some selected states and the total wound integral κ are listed for $k_F=1.65$ fm^{-1}, $k_0=0.57\,k_F$ and $P=0.3\,k_F$. The value of $\kappa_{02}^{(110)}$ is proportional to the probability of the excitation

Table V. Wound integrals $\kappa_{ll'}^{(JST)}$ and the total wound integral κ at $k_F=1.65\,\mathrm{fm}^{-1}$, $k_0=0.57k_F$ and $P=0.3k_F$ for each kind of OBEP.

	$\kappa_{00}^{(001)}$	$\kappa_{00}^{(110)}$	$\kappa_{02}^{(110)}$	$\kappa_{11}^{(011)}$	$\kappa_{11}^{(111)}$	total κ
OBEG(R)-SC	0.0158	0.0170	0.0346	0.0053	0.0113	0.0902
OBEG(NR)-SC	0.0218	0.0184	0.0204	0.0060	0.0109	0.0844
OBEG(R)-LC	0.0036	0.0029	0.0341	0.0046	0.0104	0.0606
OBEG(NR)-LC	0.0083	0.0044	0.0231	0.0051	0.0100	0.0563
OBEV(R)	0.0060	0.0065	0.0220	0.0049	0.0100	0.0534
OBEV(NR)	0.0074	0.0079	0.0203	0.0050	0.0100	0.0550

from the hole state ($<k_F$) to the particle state ($>k_F$) through the tensor interaction. The larger value of (R) than that of (NR), thus, indicates the strong tensor potential of (R) in the ${}^3E$ state. In the case of OBEV, the total wound integral κ is small reflecting smoothness of OBEV in short-range regions.

3.3. *Neutron matter properties*

To explain the structure of neutron star, it is necessary to construct the equation of state that is applicable to a wide range of density.[12] Corresponding to the increasing density with depth of a neutron star, various phases of matter form the concentric structure of star. Due to the small wound integral and the convergence of the pair expansion, the Brueckner theory is considered to be applicable to a density region $\rho=0.5\times10^{14}\sim6.0\times10^{14}\,(\mathrm{g/cm^3})$ in which there exists dense neutron gas with a small fraction of proton and electron.

In this subsection, we calculate the properties of neutron matter in this dense neutron gas region by employing the Brueckner theory with our OBEP's, in order to see the potential feature in the short-range region in $T=1$ state.

The total energy per particle and partial wave contribution from OBEP versus density are shown in Fig. 7. The results from OBEG(R) are in good agreement with those from the p-space OBEP by Bleuler et al.[13] The OBEV is slightly repulsive for higher densities, yet the differences among three kinds of OBEP with different cores are rather small compared with those of nuclear matter. Besides, the difference between (R) and (NR) are also small, which differs from the situation of nuclear matter. It should be noticed that the ${}^3P_2$ state is strongly attractive at higher densities, which allows us to expect the ${}^3P_2$ superfluidity of neutron matter.[14]

Total wound integrals κ for $k_F=2.5\,\mathrm{fm}^{-1}$, $k_0=0.57\,k_F$ and $P=0.3\,k_F$ are 0.1099, 0.0671 and 0.0753 for OBEG(R)-SC, OBEG(R)-LC and OBEV(R), respectively. In spite of its high density, the values of wound integral of neutron matter are small. This is due to the lack of ${}^3S_1+{}^3D_1$ states which have brought the large wound integral $\kappa_{02}^{(110)}$ to the case of nuclear matter. The wound integral of OBEV is larger than that of OBEG-LC contrary to the case of nuclear matter, which indicates the growth of velocity-dependent core in the high density region.

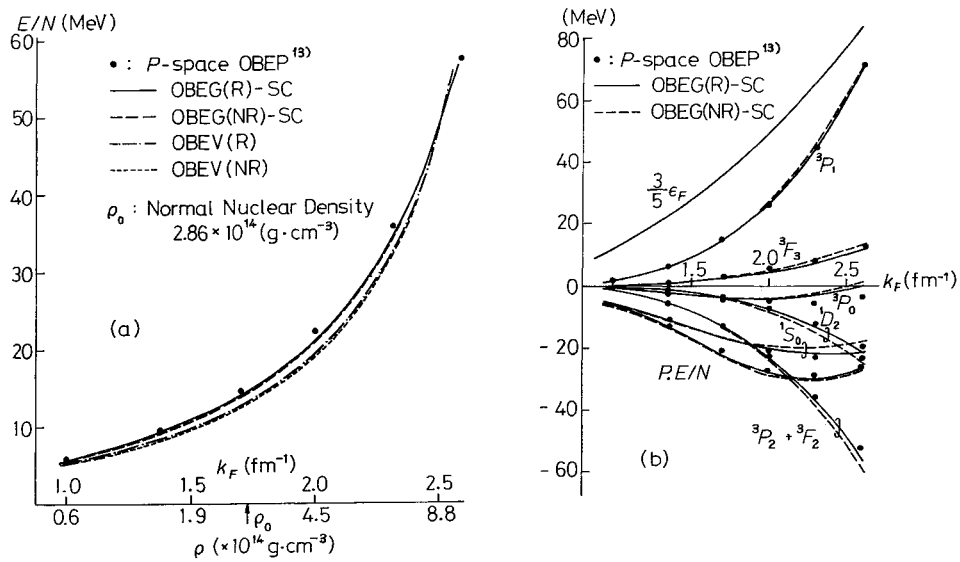

Fig. 7. Energy (a) and partial wave contributions ($l \leq 3$) (b) versus density curves obtained from our OBEP's ($\rho = 0.565 \times 10^{14} k_F^3$). $P.E/N$ indicates the total potential energy per particle and $3\epsilon_F/5$ is the kinetic energy.

§ 4. Concluding remarks

In this paper, nonstatic r-space OBEP's that include the retardation and the velocity-dependent tensor terms in addition to the other nonstatic terms of order up to $\boldsymbol{p}^2/M^2$ are constructed. The "extended Green's method" is found to be useful to treat easily the potential with velocity-dependent tensor terms.

We may conclude that the retarded effect of the OBEP in many-nucleon system plays a more important role than that in two-nucleon system. Then the nuclear potential with retardation should be employed in calculations of the finite nuclei. Accordingly, it is of interest to elucidate the retarded effect in three- and four-nucleon systems by using our OBEP's.

In spite of the limitation for treatment of nonstatic effects in coordinate space, our r-space OBEP's seem to be one of the most accurate and reliable potentials. The results predicted by our r-space OBEP with retardation on two-nucleon and many-nucleon systems are qualitatively in agreement with those clarified by the p-space OBEP.

However, in order to discuss accurately the absolute values of the retarded effects and relativistic effects in nuclear systems, it is appropriate to treat these problems throughout in momentum space. Such problems are in progress for the subject of our work.

Acknowledgements

The authors wish to thank Professor H. Tanaka for a number of important suggestions. Thanks are also due to Professor Y. Akaishi and Mr. T. Kasahara for valuable discussions on the properties of nuclear matter and neutron matter and on the calculational method of these systems. The authors would like to express their thanks to Professor R. Tamagaki for valuable discussions.

Numerical calculations were carried out by HITAC 8800/8700 at the Computer Center of the University of Tokyo, HITAC 8450 at the Computer Center of the College of Science and Technology of Nihon University and FACOM 230-60 at Hokkaido University Computing Center.

Appendix

We exhibit our nonstatic OBEP obtained in I. The OBEP is constructed by the usual Yukawa potential V_i and the retarded potential W_i, where $i=C$, T, LS, W and LL. Here we use the following abbreviations:

$$E=e^{-x},\quad Y=e^{-x}/x,\quad X=(1/x+1/x^2)\,Y,\quad Z=(1+3/x+3/x^2)\,Y,$$

$$\nabla^2 f(x)+f(x)\nabla^2=(\nabla_l^2+\nabla_r^2)f(x).$$

1) *Scalar meson*

$$V_c=-m_s g_s^2[(1-m_s^2/4M^2)\,Y+(1/2M^2)\,(\nabla_l^2+\nabla_r^2)\,Y], \tag{A1·1}$$

$$V_{LS}=-m_s g_s^2(m_s^2/2M^2)\,X, \tag{A1·2}$$

$$W_C=m_s g_s^2[(m_s^2/8M^2)\,(E-2Y)-(1/4M^2)\,(\nabla_l^2+\nabla_r^2)\,E], \tag{A1·3}$$

$$W_{LL}=-m_s g_s^2(m_s^2/2M^2)\,X. \tag{A1·4}$$

2) *Pseudoscalar meson**) $(G_p=(m_p/2M)g_p)$

$$V_C=m_p G_p^2(\boldsymbol{\sigma}_1\cdot\boldsymbol{\sigma}_2)/3\cdot[(1-m_p^2/8M^2)\,Y-(3m_p^2/8M^2)\,(X+2Z/x^2)$$
$$+(3/4M^2)\,(\nabla_l^2+\nabla_r^2)\,(Y+X)], \tag{A2·1}$$

$$V_T=m_p G_p^2(1/3)[(1-m_p^2/8M^2)\,Z+(3/4M^2)\,(\nabla_l^2+\nabla_r^2)\,Z], \tag{A2·2}$$

$$V_W=-m_p G_p^2(m_p^2/2M^2)\,Z/x^2, \tag{A2·3}$$

$$V_{LL}=m_p G_p^2(\boldsymbol{\sigma}_1\cdot\boldsymbol{\sigma}_2)/3\cdot(m_p^2/M^2)\,Z/x^2, \tag{A2·4}$$

$$W_c=-m_p G_p^2(\boldsymbol{\sigma}_1\cdot\boldsymbol{\sigma}_2)/3\cdot[(m_p^2/8M^2)(E-2Y)-(1/4M^2)(\nabla_l^2+\nabla_r^2)E], \tag{A2·5}$$

$$W_T=-m_p G_p^2(1/3)[(m_p^2/8M^2)\,(E+Y)-(1/4M^2)\,(\nabla_l^2+\nabla_r^2)\,(E+Y+2Z)], \tag{A2·6}$$

$$W_W=m_p G_p^2(m_p^2/M^2)\,Z/x^2, \tag{A2·7}$$

*) We express only the pseudoscalar coupling case for simplicity.

$$W_{LL}=m_p G_p^{\,2}(\boldsymbol{\sigma}_1\cdot\boldsymbol{\sigma}_2)/3\cdot(m_p^{\,2}/M^2)\,(X/2-Z/x^2). \tag{A2·8}$$

3) *Vector meson (vector coupling)*

$$V_C=m_v g_v^{\,2}[(1+m_v^{\,2}/2M^2)\,Y+(\boldsymbol{\sigma}_1\cdot\boldsymbol{\sigma}_2)\,(m_v^{\,2}/6M^2)\,Y-(1/2M^2)\,(\boldsymbol{\nabla}_l^{\,2}+\boldsymbol{\nabla}_r^{\,2})\,Y], \tag{A3·1}$$

$$V_T=-m_v g_v^{\,2}(m_v^{\,2}/12M^2)\,Z, \tag{A3·2}$$

$$V_{LS}=-m_v g_v^{\,2}(3m_v^{\,2}/2M^2)\,X, \tag{A3·3}$$

$$W_C=-m_v g_v^{\,2}[(m_v^{\,2}/8M^2)\,(E-2Y)-(1/4M^2)\,(\boldsymbol{\nabla}_l^{\,2}+\boldsymbol{\nabla}_r^{\,2})\,E], \tag{A3·4}$$

$$W_{LL}=m_v g_v^{\,2}(m_v^{\,2}/2M^2)\,X. \tag{A3·5}$$

4) *Vector meson (mixing coupling)*

$$V_c=m_v g_v f_v(m_v/M)\,[Y+2(\boldsymbol{\sigma}_1\cdot\boldsymbol{\sigma}_2)/3\cdot Y], \tag{A4·1}$$

$$V_T=-m_v g_v f_v(m_v/3M)\,Z, \tag{A4·2}$$

$$V_{LS}=-m_v g_v f_v(4m_v/M)\,X. \tag{A4·3}$$

5) *Vector meson (tensor coupling)*

$$V_C=m_v f_v^{\,2}(\boldsymbol{\sigma}_1\cdot\boldsymbol{\sigma}_2)/3\cdot[(2+5m_v^{\,2}/8M^2)\,Y-(3m_v^{\,2}/8M^2)\,(X+2Z/x^2)$$
$$-(1/4M^2)\,(\boldsymbol{\nabla}_l^{\,2}+\boldsymbol{\nabla}_r^{\,2})\,(Y-3X)]+m_v f_v^{\,2}(m_v^{\,2}/4M^2)\,Y, \tag{A5·1}$$

$$V_T=-m_v f_v^{\,2}[(1/3+m_v^{\,2}/24M^2)\,Z+(1/12M^2)\,(\boldsymbol{\nabla}_l^{\,2}+\boldsymbol{\nabla}_r^{\,2})\,Z], \tag{A5·2}$$

$$V_{LS}=-m_v f_v^{\,2}(3m_v^{\,2}/2M^2)\,X, \tag{A5·3}$$

$$V_W=m_v f_v^{\,2}(3m_v^{\,2}/2M^2)\,Z/x^2, \tag{A5·4}$$

$$W_C=-m_v f_v^{\,2}(\boldsymbol{\sigma}_1\cdot\boldsymbol{\sigma}_2)/3\cdot[(m_v^{\,2}/4M^2)\,(E-5Y-6X-12Z/x^2)$$
$$-(1/2M^2)\,(\boldsymbol{\nabla}_l^{\,2}+\boldsymbol{\nabla}_r^{\,2})\,(E-3Y-6X)], \tag{A5·5}$$

$$W_T=m_v f_v^{\,2}[(m_v^{\,2}/24M^2)\,(E+Y)-(1/12M^2)\,(\boldsymbol{\nabla}_l^{\,2}+\boldsymbol{\nabla}_r^{\,2})\,(E+Y+2Z)], \tag{A5·6}$$

$$W_W=-m_v f_v^{\,2}(m_v^{\,2}/M^2)\,Z/x^2, \tag{A5·7}$$

$$W_{LL}=m_v f_v^{\,2}(\boldsymbol{\sigma}_1\cdot\boldsymbol{\sigma}_2)/3\cdot(m_v^{\,2}/M^2)\,(X-2Z/x^2). \tag{A5·8}$$

References

1) T. Obinata and M. Wada, Prog. Theor. Phys. **53** (1975), 732.
2) T. Obinata, M. Wada and T. Kasahara, Prog. Theor. Phys. **53** (1975), 1406.
3) T. Obinata and M. Wada, Prog. Theor. Phys. **52** (1974), 1394.
4) S. Otsuki, R. Tamagaki and M. Wada, Prog. Theor. Phys. **32** (1964), 220.
5) T. Obinata and M. Wada, Prog. Theor. Phys. **56** (1976), 677.
6) M. MacGregor, R. Arndt and R. Wright, Phys. Rev. **182** (1969), 1714.
7) K. Holinde, K. Erkelentz and R. Alzetta, Nucl. Phys. **A194** (1972), 161; **A176** (1971), 413.
8) M. Harada, R. Tamagaki and H. Tanaka, Prog. Theor. Phys. **36** (1966), 1003.
M. Harada, Prog. Theor. Phys. **38** (1967), 353.

9) Y. Akaishi, H. Bando, A. Kuriyama and S. Nagata, Prog. Theor. Phys. **40** (1968), 288.
10) R. Tamagaki, *Proceedings of International Conference on Nuclear Structure* (Physical Society of Japan, 1968), p. 27.
11) K. Holinde, K. Erkelentz and R. Alzetta, Nucl. Phys. **A198** (1972), 598.
12) S. Ikeuchi, S. Nagata, T. Mizutani and K. Nakazawa, Prog. Theor. Phys. **46** (1971), 95.
G. Baym, H. A. Bethe and J. Pethick, Nucl. Phys. **A175** (1971), 225.
A. Hewish, Rev. Mod. Phys. **47** (1975), 567.
13) K. Bleuler, K. Erkelentz, K. Holinde and R. Machleidt, Nucl. Phys. **A205** (1973), 292.
14) R. Tamagaki, Prog. Theor. Phys. **44** (1970), 905.
T. Takatsuka and R. Tamagaki, Prog. Theor. Phys. **46** (1971), 114.